Functional imaging and targeted drug delivery in mice and patient tumors with a cell nucleolus-localizing and tumor-targeting peptide

Renwei Jing
Tianjin Medical University
Qian Wang
Tianjin Medical University
Lu Chen
Tianjin Medical University
Guangtao Li
Tianjin Medical University
Ruibin Li
Tianjin Medical University
Leijie Zhang
Tianjin Medical University
Hongbing Zhang
Tianjin Medical University General Hospital
Bingfeng Zuo
Tianjin Medical University
Yiqi Seow
Institute of Bioengineering and Bioimaging, Singapore
Xin Qiao
Tianjin Medical University
Jingyuan Xu
Tianjin Medical University
Jun Chen
Tianjin Medical University General Hospital
Tianqiang Song
Tianjin Medical University
HaiFang Yin (haifangyin@tmu.edu.cn)
Tianjin Medical University

Research Article

Keywords: Tumor, HCC, tumor-targeting and cell nucleolus-localizing peptide, chemotherapy

Posted Date: April 21st, 2022

DOI: https://doi.org/10.21203/rs.3.rs-1567587/v1

Abstract

Tumor-targeting peptides have profound clinical implications in early detection and delineation of microscopic lesions for surgical resection, and also delivery of therapeutics with reduced systemic toxicity. Here, we demonstrate that a peptide (RS), selected from a rationally-designed variant library of a reported hepatocellular carcinoma (HCC)-targeting peptide P47, enables discrimination of HCC from noncancerous tissues in orthotopic HCC mice and patient biopsies, and delineation of micrometastases in lung, with up to 21-fold contrast between tumor and surrounding liver, significantly higher than P47. Importantly, RS targets non-small cell lung (NSCLC) and colon cancers in mice and patient biopsies, with higher selectivity for highly proliferative tumor nodules. Moreover, RS localizes to cell nucleoli of HCC, NSCLC, breast, colon and cervical cancer cells and induces cell nucleolar stress when conjugated with chemotherapeutic Oxaliplatin (OXA) (RS-OXA), demonstrating both cellular and subcellular targeting. RS-delivered OXA elicits significant tumor retardation in orthotopic HCC mice with markedly reduced systemic toxicity compared to OXA alone. Injection of fluorescence-labeled RS enables dynamic visualization of tumor growth in RS-OXA-treated subcutaneous HCC mice. Our study demonstrates that RS targets a spectrum of tumors and localizes to cell nucleolus, and enables functional imaging and targeted delivery of OXA in HCC mice, and thus provides a versatile tool for tumor imaging and targeted therapeutics.

Introduction

Tumor-targeting peptides show potential in tumor imaging and targeted therapy due to low molecular weight, small size, high affinity and selectivity, low toxicity and production cost.[1, 2] A myriad of tumor-targeting peptides have been identified and extensively tested as molecular probes for tumor imaging or surgical navigation and cancer treatment in preclinical studies.[3–6] Examples include an internalizing-RGD peptide that specifically targets glioblastoma, melanoma, lung, prostate and breast cancer by binding to αvβ3 integrin on tumor cell surfaces.[7], [8, 9] NGR that targets CD13 on endothelial cells of colorectal, ovarian, non-small-cell lung cancer (NSCLC), small-cell lung cancer (SCLC) and hepatocellular carcinoma (HCC)[10, 11] has been tested in clinical trials.[12] However, none of them shows the ability to enter tumor cell nucleoli.

As a non-membrane-bound sub-nuclear structure and a factory for ribosome biogenesis, [13], [14] the cell nucleolus represents a promising subcellular therapeutic location as hyperactive ribosome biogenesis was shown to contribute to aggressiveness and resistance of cancers.[15] Probes tracking cell nucleolus have been extensively explored but most of them lack tumor-targeting property.[16, 17] Moreover, multidrug resistance (MDR) induced by ATP-binding cassette (ABC) transporters on plasma membrane and systemic toxicity are the major hurdles for chemotherapeutic treatment of cancers,[18, 19] specific delivery of chemotherapeutic drugs to tumor and cell nucleolus can avoid these issues. Therefore, approaches to target tumor and cell nucleolus have the potential to unlock the full potential of tumor chemotherapy with manageable safety risks, particularly in difficult-to-treat tumors such as HCC.

HCC is highly refractory to conventional chemotherapy,[20] due to its high pathological heterogeneity and high metabolic activity.[21] Several oxaliplatin (OXA)-based regimens resulted in improved response rates and survival benefits compared to doxorubicin and other platinum-based chemotherapeutic drugs in clinical trials for advanced HCC;[22] however OXA therapy suffered from severe drug-related adverse effects including systemic toxicity and MDR after repeated doses.[23, 24] Moreover, OXA was shown to effect nucleolar or ribosome biogenesis stress rather than trigger DNA damage response, unlike other platinum-containing chemotherapeutic agents.[25, 26] Thus, tumor- and cell nucleolus-targeted delivery of OXA is critical for antitumor efficacy on tumor cells.

Previously, we identified a HCC-targeting peptide (P47) that enabled detection of tumor micronodules in mice and patients with HCC; [27] however, it showed limited effect on other tumors and was unable to enter cell nuclei. To improve its ability to target a large spectrum of tumors and cell nuclei, particularly, cell nucleolus, we rationally designed 384 peptide variants based on P47 sequence with a bioinformatics tool (http://crdd.osdd.net/raghava/tumorhpd). Among predicted peptide variants, RS outperformed P47 and other variants and showed greater specificity for HCC, NSCLC and colon cancers over peritumoral tissues in mice and patient biopsies, and improved targeting ability to NSCLC, breast, colon and cervical cancers in mice. Importantly, RS effectively localized to cell nucleolus of HCC, NSCLC, breast, cervical and colon cancers, a property was not observed with P47. RS directed HCC-targeted delivery and cell nucleolus localization of OXA *in vitro* and in orthotopic HCC mice when conjugated with OXA (RS-OXA), with significantly reduced systemic toxicity. Dynamic monitoring of tumor growth was achieved when fluorescence-labeled RS were simultaneously injected in RS-OXA-treated subcutaneous HCC mice. Our study demonstrates that RS enables clear discrimination of a variety of tumors from peritumoral tissues in mice and patients and directs tumor- and cell nucleolus-specific delivery of OXA in HCC mice, and thus provides a new tool for tumor imaging and targeted therapy.

Results

Rationale design identifies lead peptide with strong HCC-targeting ability

To enhance the tumor-targeting and cell-permeabilizing ability of P47,[27] we employed a bioinformatics tool (http://crdd.osdd.net/raghava/tumorhpd/ and https://webs.iiitd. edu.in/raghava/tumorhpd/), a TumorHPD web server for tumor-homing peptide prediction,[28] to identify P47 variants with stronger tumor-targeting and cell- permeabilizing ability based on their support vector machine (SVM) scores, hydrophilicity or solubility, charge and isoelectric point (pI).[29] To determine which end is more important for its targeting ability, we coupled FAM to different ends of P47 and administered the peptides to subcutaneous HCC mice. Weaker fluorescence signals were detected in tumor with FAM coupled to the C terminus than the N terminus (Figure S1a), indicating that the C terminus may be more important. Thus, mutations were largely introduced to the N terminus of P47. Systemic intravenous injection of top two variants with similar SVM scores revealed significantly stronger fluorescence signals with FAM-labeled V2 than V1 and P47 peptides in tumor of subcutaneous HCC mice under identical conditions (Figure 1a-c). Based on the strong tumor-targeting efficacy of V2, we generated more V2 mutants. Strikingly, more

specific tumor accumulation was observed with V2-RS in subcutaneous HCC mice (tumor-liver ratio of 28.37±0.80) than P47 (8.24±0.80) (Figure 1b and 1c), demonstrating a stronger HCC-targeting potency of V2-RS (RS). Consistently, although V2-RK, -RA, or -RL showed slightly higher SVM scores than RS, there was no further improvement compared to parental V2 (Figure 1b and 1c).

To investigate RS in a more clinically relevant setting, we intravenously administered FAM-labeled RS and P47 in orthotopic HCC mice at the dose of 25 mg/kg for single injection. Although both RS and P47 were able to clearly delineate the margin between tumor and surrounding tissues, RS showed stronger fluorescence signals and higher tumor-liver contrast (21.22 ± 0.97) than P47 (7.56 ± 0.36) (Figure 1d), a difference similar to that of subcutaneous HCC mice. As micrometastases largely account for post-surgical recurrence, [30] we examined the effect of RS on lung micrometastasis in HCC mice in by intravenously injected Hepa1-6 cells to wild-type mice.[31] Remarkably, RS labeled metastatic HCC micronodules of 0.1mm in diameter in lungs of mice (Figure 1e). In contrast, P47 was only able to mark micronodules with a diameter of 0.3mm in HCC mice bearing metastatic mCherry-expressing tumors in lungs (Figure S1b). As detection of deeply-located HCC nodules is typically challenging during surgery, [32] to investigate the feasibility of visualizing tumor nodules deep inside the liver, we labeled RS with quantum dot (Ag_2S-RS) and intravenously injected Ag_2S-RS in orthotopic HCC nude mice bearing human HCC tumors at the dose of 4mg/kg. Both deeply-located and superficial tumor micronodules were clearly highlighted with Ag_2S-RS (Figure 1f), confirming the sensitivity and specificity of RS. Notably, RS showed high serum stability than P47, [27] with 71.8% of the peptide remained intact in 20% serum at 8 h, as revealed by liquid chromatography-electrospray mass spectrometric (LC-MS) analysis (Figure 1g). Similar to P47, [27] RS was also sequentially degraded from the C terminus (Figure 1g). Moreover, intravenous injection of RS at high dose (100mg/kg) did not induce any detectable toxicity in wild-type mice reflected by levels of aspartate aminotransferase (AST) and alanine aminotransferase (ALT) (Figure S1c) and normal morphological structures of liver and kidney (Figure S1d). Altogether, these findings demonstrated that RS targets HCC with high sensitivity, specificity and serum stability.

RS discriminates tumor from peritumoral tissue in HCC and ICC patient biopsies

To investigate the clinical applicability of RS in differentiating tumor from abnormal liver in HCC patients, we applied FAM-labeled RS to surgically excised fresh tumor and peritumoral liver tissues. Clear delineation of tumor margins or microscopic lesions from surrounding tissues was achieved in HCC patient biopsies with FAM- labeled RS, with microscopic lesions of 0.1mm in diameter (Figure 2a) and residual tumor tissues after surgery being highlighted (Figure S2). RS was also able to detect tumor infiltration in the liver of HCC patients (Figure 2b), a phenomenon frequently observed in HCC patients. [33] Importantly, RS enabled the discrimination of HCC tumors with high or low proliferative activities, characterized by the abundance of ribosomes and size of nucleoli,[34] with substantial accumulation in highly proliferative tumor nodules (Figure 2c), implying that RS might target with efficacy proportional to tumor aggressiveness. Consistently, a much weaker fluorescence signal was found in hemorrhagic necrosis areas of HCC tissues with low proliferative activity, manifested by karyorrhexis and karyolysis, [35] than other areas in HCC patient biopsies (Figure 2d). Strikingly, RS demonstrated clear differentiation

of tumor from highly heterogeneous surrounding liver tissues including normal-like liver, lipid degeneration, inflammation, fibrosis, cirrhosis and nodular hyperplasia when HCC patient biopsies were assembled in order of disease progression, confirmed by histological analysis (Figure 2e), strengthening the therapeutic potential and general applicability of RS in HCC patients at different stages. Moreover, RS discriminated intrahepatic cholangiocarcinoma (ICC) with proliferative bile ducts from peritumoral liver tissues with severe inflammatory infiltration in patient biopsies (Figure 2f). Clear differentiation of ICC and HCC in the combined ICC-HCC patient cases was observed in a highly heterogeneous background including moderate lipid degeneration, inflammatory infiltration and bile duct proliferation (Figure 2g), with a comparable tumor-liver ratio between ICC and HCC (Figure 2h), demonstrating the clinical applicability of RS in detecting HCC and ICC.

RS targets different tumors in mice and patient biopsies

To examine whether RS is able to target other tumors besides HCC, we intravenously administered FAM-labeled RS into nude mice bearing subcutaneous human non-small cell lung (NSCLC), breast, cervical and colon tumors. Strikingly, RS specifically accumulated in tumors of different types, with HCC ranking top and NSCLC and colon cancer secondary to HCC based on the ratio of tumor relative to corresponding tissues (Figure 3a and 3b). Unsurprisingly, a clear delineation of tumor from peritumoral lung tissues was achieved in mice bearing orthotopic murine and human NSCLC, with a tumor/ lung ratio of 6.31±1.12 and 8.24±0.49, respectively (Figure 3c). Correspondingly, RS clearly differentiated lung adenocarcinoma from peritumoral lungs with infiltrating monocytes, pneumoconiosis and fibrosis in patient biopsies (Figure 3d and 3e). Importantly, RS enabled marked discrimination of highly proliferative lung adenocarcinoma, characterized by papillary or micropapillary structures and high nucleo-cytoplasmic ratio,[36] from less proliferative tumors, reflected by the appearance of simple acinar structures,[37] in patient biopsies, with a significantly greater tumor/ lung ratio in highly than less proliferative lung adenocarcinoma (Figure 3e), including the hemorrhagic necrosis area of lung adenocarcinoma tissues (Figure 3f). A similar pattern was observed in lung squamous carcinoma, with RS showing stronger fluorescence signals in highly proliferative, represented by clustered tumor cells with high nucleo-cytoplasmic ratio[38], than poorly proliferative tumors (Figure 3g), characterized by the formation of keratin pearl at the center of cancer nest.[39] Similarly, RS also distinguished colon adenocarcinoma from peritumoral colon tissues in patient samples with similar indications as NSCLC and HCC (Figure S3). These data showed that RS targets a broad spectrum of tumors with selectivity for highly proliferative tumor nodules.

RS specifically localizes to tumor cell nucleolus

Considering RS's broad tumor-targeting ability, we wondered whether RS can be readily internalized by different tumor cells. Substantially stronger fluorescence signals were observed in human HCC cells treated with FAM-labeled RS than P47, with faint signals found in noncancerous human hepatocytes (Figure 4a and 4b). As expected, significantly greater cellular uptake was yielded in human NSCLC, colon, breast and cervical cancer cells treated with FAM-labeled RS, whereas negligible levels were detected with P47 under identical conditions (Figure 4a-c), indicating the potent tumor cell internalization capacity of

RS. Strikingly, stronger fluorescence signals were found in cell nuclei, with punctate foci in cell nucleoli, of human HCC cells treated with FAM-labeled RS. P47 predominantly localized in cytoplasm with small amounts scattered in nuclei[27] (Figure 4d). Similar observations were detected in other human HCC and tumor cells, with substantial amounts of RS accumulated in cell nucleoli (Figure 4e), confirming the strong tumor cell nucleolus-localizing capacity of RS.

RS augments OXA's specific uptake and cytotoxicity in HCC cells *in vitro*

RS's tumor-targeting and cell nucleolus-localizing properties could be therapeutically useful, thus we assessed RS-mediated delivery of OXA, a first-line chemotherapeutic agent for HCC patients with primary effects in cell nucleolus.[25] RS-OXA with 96.43% purity and molecular weight of 1928.84 was synthesized (Figure S4a and S4b). Remarkably, strong fluorescence signals were observed in tumor cell nucleolus when AF680-labeled RS-OXA was incubated with human HCC cells, but not in noncancerous human hepatocytes (Figure 5a), indicating tumor cell nucleolus-specific uptake of OXA. As OXA primarily induces nucleolar stress,[25, 26] we examined the translocation of nucleophosmin (NPM1), an indicator for nucleolar stress characterized by translocation from cell nucleoli to nucleoplasm in response to stress, [26] in human HCC cells. As expected, NPM1 was largely diffused in cell nucleoplasm of HCC cells treated with RS-OXA, whereas the expression of NPM1 appeared as punctate foci in cell nucleoli of PBS- or OXA-treated HCC cells (Figure 5b). In clear contrast, no evident NPM1 expression was detected in nucleoplasm of noncancerous hepatocytes treated with either RS-OXA or OXA (Figure 5b), demonstrating that RS promotes HCC- and cell nucleolus-specific uptake of OXA and results in nucleolar stress. Correspondingly, significantly higher rates of cellular apoptosis, reflected by annexin V and propidium iodide (PI) double staining [40] (Figure 5c and 5d), and cytotoxicity (Figure 5e) were triggered by RS-OXA than by OXA in human HCC cells. Notably, RS-OXA had a much less impact on human noncancerous hepatocytes than OXA (Figure 5c-e). Unsurprisingly, human HCC cell invasion ability was also dramatically compromised by RS-OXA, to a much less extent with OXA, whereas no migratory inhibition was observed with RS-OXA-treated human noncancerous hepatocytes (Figure 5f). However, OXA induced a significant inhibitory effect on cell migration in human noncancerous hepatocytes (Figure 5f), indicating the nonspecific cell toxicity. These results demonstrated that RS augments OXA's tumor- and cell nucleolus-specific uptake, resulting in cell nucleolar stress, cytotoxicity and migratory inhibition *in vitro*.

RS enables tumor detection and specific OXA delivery in HCC mice

To investigate the ability of RS to direct tumor-specific delivery of OXA *in vivo*, we intravenously administered RS-OXA into day-7 subcutaneous HCC mice at the dose of 10 μmol/kg for 5 times every 3 days apart (Figure 6a), a dosing regimen adopted from previous studies.[41] As real-time monitoring of the therapeutic effect of drugs is critical for clinical assessment, we injected AF680-labeled RS intravenously at the dose of 500 μg/kg at different time-points and examined mice 12 h later (Figure 6a). RS-OXA significantly inhibited tumor growth compared to OXA alone under identical conditions (Figure 6b and 6c). Importantly, AF680-labeled RS enabled dynamic visualization and clear delineation of tumors in pretreated and treated tumor- bearing mice (Figure 6b and 6c), indicating the potential of RS for targeted

therapeutic intervention and prognostic monitoring. Consistently, RS-OXA triggered sustainable tumor suppression in day-7 orthotopic HCC mice under identical dosing conditions (Figure 6d), reflected by significant tumor retardation in RS-OXA-treated mice compared to OXA-treated and untreated mice (Figure 6e and 6f), demonstrating the specific antitumor potency of RS-OXA. Strikingly, RS-OXA also prevented pulmonary metastasis in orthotopic HCC mice, whereas prominent metastasis was found in mice treated with OXA and untreated controls (Figure 6g). Notably, no morphological changes were observed in kidneys across different treatment groups (Figure S4c), which is consistent with previous reports on OXA.[42] Corroborating with negligible adverse effects observed with RS- OXA, significantly higher amounts of Pt accumulated in tumor of mice treated with RS-OXA than OXA, whereas negligible in surrounding liver tissues (Figure 6h). In contrast, comparable levels of Pt were found in tumor and liver tissues of mice treated with OXA (Figure 6h). Importantly, RS-OXA did not evoke any acute neuropathy, an adverse effect frequently occurred with OXA treatment,[43] reflected by significantly less neuropathic pain in nude mice treated with RS-OXA than OXA and comparable to untreated controls when exposed to cold (Figure 6i). Also sinusoidal obstruction syndrome (SOS), a liver parenchymal damage primarily involving sinusoids,[44] was markedly reduced in liver of nude mice treated with RS-OXA compared to OXA (Figure 6j). Moreover, tumor-targeted delivery of OXA reduced its adverse effect on bodyweight loss of nude mice (Figure S4d). Altogether, these findings confirmed that RS directs tumor-targeted delivery of OXA, and resulting in sustainable tumor inhibition with improved safety profiles.

Discussion

One of major goals for molecular imaging is the ability to characterize microscopic lesions *in vivo* to avoid the added risks associated with the removal of benign surrounding tissues.[44] Likewise, targeted delivery of chemotherapeutic agents to malignant cells, particularly to cell nucleolus, is able to minimize systemic toxicity and potential drug resistance related to ATP-binding cassette (ABC) transporters on plasma membrane.[15] Here, we identified a peptide (RS) that enables clear delineation of tumor from peritumoral tissues in mice and patient biopsies of HCC, ICC, NSCLC and colon cancers, with higher selectivity for actively proliferating tumor cells in patient biopsies. Importantly, RS specifically localized to cell nucleolus and mediated tumor- and cell nucleolus-specific delivery of OXA, resulting in tumor cell nucleolar stress and cytotoxicity *in vitro* and significant tumor suppression in HCC mice, with markedly reduced adverse effects and systemic toxicity. Injection of fluorescence- labeled RS enabled dynamic monitoring of tumor growth and drug efficacy in HCC mice treated with RS-OXA. Our study provides a new tool for functional imaging and targeted drug delivery in a wide array of cancers.

Although OXA has been extensively used a front-line treatment for different cancers, particularly for HCC,[22] one major hurdle for the clinical implementation of OXA is systemic toxicity.[43] In our current study, we tagged OXA with RS and achieved tumor- and cell nucleolus-specific delivery of OXA, yielding augmented therapeutic efficacy with minimal systemic toxicity in HCC mice. Worthy mentioning, RS can be routinely synthesized and scaled up at low costs, and conjugation with OXA does not require sophisticated chemical techniques, thus it is likely that RS-OXA can be manufactured easily and fast-tracked to the clinic upon completion of extensive toxicological and pharmacokinetic studies of RS.

Although we did not detect any liver or kidney toxicity in mice at tested doses, safety studies in large animals at higher doses are essential prior to clinical deployment of RS. In addition, multi-drug resistance elicited by ATP-binding cassette (ABC) transporters on plasma membrane is another critical issue for chemotherapy,[18] RS-mediated cell nucleolus-specific drug delivery can potentially overcome this and extensive studies on this aspect are warranted in future.

Post-surgical recurrence is a common phenomenon in tumor including HCC, lung and colon and other cancers.[45–47] Among them, HCC ranks top with 70.2% recurrence rate within 84.4 months after surgery.[48] Given high recurrence rates are closely associated with the failure to detect micrometastases with current imaging techniques; [49] there is a clear need to identify molecular probes with higher sensitivity and specificity. The ability of RS to detect microscopic lesions with a diameter of 0.1mm would greatly enhance detection of micrometastases and facilitate surgical navigation and reduce chances of surgical recurrence, potentially increasing 5-year survival rates of HCC, by extension to other cancer patients. Importantly, we demonstrated that RS can differentiate tumor nodules of different proliferative activities, with higher selectivity for highly proliferative tumor nodules. This unique feature can be exploited to target the remaining post-surgical micrometastases, which are largely highly proliferative and the main contributors to the recurrence.[30] By incorporating RS to imaging tracers of positron emission tomography (PET) to pinpoint microscopic lesions with high proliferative activities, RS can be used to guide local radiotherapy and other interventions and also to predict tumoral response. Therefore, our findings may have significant implications for surgical navigation or post-surgical monitoring and PET-guided targeted therapy.

In summary, we demonstrated that RS targets a broad spectrum of tumors with high sensitivity and specificity and localizes to cell nucleolus and RS-mediated tumor- and cell nucleolus-specific delivery of OXA significantly enhances OXA's activity with minimal systemic toxicity in HCC mice, thus providing a new tool for functional imaging and targeted drug delivery.

Conclusions

In summary, we identified a peptide (RS), which targets a spectrum of tumors and localizes to cell nucleolus and enables functional imaging and targeted delivery of OXA in HCC mice, and thus provides a versatile tool for tumor imaging and targeted therapeutics in a variety of tumors.

Materials And Methods

Animals and injections

C57BL/6 wild-type and *BALB/C* nude mice (6-8-week old) were used in all experiments (the number used was specified in Figure legends). Mice were housed under specific pathogen free conditions in a temperature-controlled room. The experiments were carried out in the Animal unit, Tianjin Medical University (Tianjin, China), according to procedures authorized by the institutional ethical committee

(Permit Number: SYXK 2019-0004). Mice were sacrificed by CO_2 inhalation or cervical dislocation at desired time-points, and tissues were fixed with Bouin's solution (Sigma, St. Louis, MO, US) and embedded with paraffin for immunohistochemical and histological studies.

OXA or RS-OXA was dissolved in N,N-dimethylformamide (DMF)/ Tween 80/ PBS (5:1:94, volumetric ratio) and injected intravenously at the dose of 10μmol /kg into mice bearing subcutaneous or orthotopic HCC tumors for 5 times every 3 days apart. The length (L) and width (W) of subcutaneous HCC tumor were measured with a caliper at 7, 10, 14, 17 and 21 days after tumor implantation. Tumor size was calculated by the formula: $(L\times W^2)/2$. While tumor size of orthotopic HCC tumor was calculated based on MRI images at 1, 2, and 3 weeks after tumor implantation. For real-time monitoring of the therapeutic effect of RS-OXA, AF680-labeled RS peptides were intravenously injected into subcutaneous HCC mice 12 h prior to imaging with the IVIS spectrum imaging system (PE, Waltham, MA, US).

Clinical samples

The hepatocellular carcinoma (HCC), intrahepatic cholangiocarcinoma (ICC), combined HCC and ICC, colon adenocarcinoma (CA) and NSCLC patient biopsies used in this study were provided by Tianjin Medical University General Hospital and Cancer Hospital (Permit Number: bc2020175). All patients provided written informed consent for the sample collection. This study was conducted in accordance with Declaration of Helsinki and was approved by the Tianjin Medical University Cancer Hospital Ethics Committee.

Establishment of tumor-bearing mouse models

To establish mouse models bearing subcutaneous tumors, MHCC-LM3 (5×10^5), Hepa1-6 (1×10^6), A549 (1×10^6), HCT116 (1×10^6), MDA-MB-231 (1×10^6) and Hela (1×10^6) cells were suspended in 70 μl PBS and injected into *C57BL/6* or *BALB/C* nude mice subcutaneously. For orthotopic HCC mice, subcutaneous tumors with a longitudinal diameter of 1cm were collected from subcutaneous mice after CO_2 inhalation or cervical dislocation. Tumor tissues were washed in D-hanks buffer and necrotic tumor tissues were removed and remaining tumor tissues were cut into about $1mm^3$ pieces. The recipient mice were anesthetized with isoflurane and skin was sterilized with iodophor 3 times before surgery as described previously.[31] Tumor tissues (3-5 pieces) were implanted in the left lobe of liver in the recipient mice under anesthesia, and the peritoneum and skin were closed with 4-0 sutures. For HCC mice bearing lung metastasis, 1×10^6 MHCC-LM3 cells were suspended in 100 μl PBS and intravenously injected into *BALB/C* nude mice within 5 seconds. For mice bearing orthotopic murine and human NSCLC, LLC1 (1×10^6) or A549 (1×10^6) cells were suspended in 100 μl PBS and intravenously injected into *C57BL/6* or *BALB/C* nude mice within 5 seconds.

Cellular uptake

Peptides were synthesized and purchased from China Peptides (Shanghai, China) with purity higher than 95%. HL7702, MHCC-97H, Hep3B, MHCC-LM3, HCT116, A549, MDA-MB-231 and Hela cells (10^4 cells/well) were cultured in serum-free medium for 2 h prior to the addition of FAM-labeled P47 or RS peptides (2 μM) and incubated for another 6h. Cells were washed with PBS for 5 times and observed with fluorescence microscope (IX70, Olympus, Tokyo, Japan). Flow cytometry (BD FACS Calibur, Franklin Lakes, NJ, US) was used for measuring cellular uptake and data were analyzed with the software FlowJo (Tree Star Inc., Ashland, OR, US). To examine the co-localization, FAM-labeled P47 or RS-treated cells were fixed with 4% PFA and counter-stained with DAPI for 15 minutes at room temperature (RT), followed by observation with a confocal laser scanning microscope (LSM700, Carl Zeiss, Germany) with a 40× objective lens.

Serum stability assay

The RS peptide (1 mM) was mixed with 20% mouse serum at a volume ratio of 4:1 and incubated at 37°C for different time-points (0 minute, 1 h, 2 h, 4 h or 8 h). 100 mM dithiothreitol (DTT) was added to reduce the formation of disulfide bonds. Trichloroacetic acid (TCA, 10%) was used to precipitate serum proteins. Subsequently, the solution was cooled at -20°C for at least 20 minutes and centrifuged at 6000g for 10 minutes, and then the supernatants were collected for liquid chromatography-mass spectrometry (LC-MS) analysis (Agilent 7500ce, Agilent Technologies, Waldbronn, Germany).

In vitro binding assay

Fresh HCC, ICC, combined HCC and ICC, CA and NSCLC patient biopsies including tumors and peritumoral tissues were incubated with 10 μM FAM-labeled RS peptides for 30 minutes at 37℃, followed by washing with PBS 5 times for 2 minutes each time. Then the tumor and peritumoral tissues were imaged with the IVIS spectrum imaging system (PE, Waltham, MA, US).

Tissue distribution

FAM-labeled peptides were diluted in 150 μl PBS and administered into *C57BL/6* or *BALB/C* nude mice bearing subcutaneous or orthotopic HCC, NSCLC, CA, breast and cervical cancers intravenously at a dose of 25 mg/kg. Treated mice were terminally anesthetized 2 h post-injection and perfused with 50 ml of cold PBS to wash out unbound peptides. Brain, quadriceps, lung, spleen, kidney, heart, liver, tumor and lung metastases were harvested for imaging with IVIS spectrum imaging system (PE, Waltham, MA, US). RS modified Ag_2S quantum dots (RS-Ag_2S) was diluted in 150 μl PBS and intravenously administered into *BALB/C* nude mice bearing orthotopic HCC at a dose of 10 mg/kg. The liver of treated mice was imaged 6 h after injection with a NIR-II image system developed by Institute of Automation (Chinese Academy of Sciences, Beijing, China). This system has two CCD cameras: an electron- multiplying CCD (EMCCD) was used to collect NIR-II fluorescent images (ProEM, Princeton Instrument, US); another color CCD was used to collect visible color images (Pilot piA1400-17gc, Basler, Germany). Illumination was provided by a light emitting diode (LED) (NIR light source, center wavelength 808 nm, maximum power

20W) for RS-Ag_2S excitation and a 150W halogen lamp (KL1500LCD, SCHOTT, Germany) for white light color imaging.

Immunohistochemistry and histology

RS was diluted in 150 μl PBS and administered into *C57BL/6* mice at a dose of 50 mg/kg. Mice were sacrificed 24 h after injection and liver/ kidney were harvested for histological examination. Serum was collected from the jugular vein for analysis of serum aspartate aminotransferase (AST) and alanine aminotransferase (ALT) (Clinical pathology laboratory, Tianjin Metabolic Disease Hospital, Tianjin, China). Routine H&E staining was used to examine the morphology and pathology of liver, lung, kidney, HCC tumor, lung metastases and clinical tissues. Briefly, tissues were fixed in Bouin's solution (Sigma, St. Louis, MO, US), embedded with paraffin and cut into 8 μm-thick sections. Subsequently, slides were baked at 60°C for 1 h and then taken through xylene and graded ethanols into distilled water, followed by incubation in filtered 0.1% Mayers Hematoxylin for 10 minutes for nucleus staining. And sections were rinsed in cool-running water to remove excessive hematoxylin, and treated with 0.5% hydrochloric acid and sodium bicarbonate solution (1%), respectively, followed by incubation in 0.5% eosin (0.5g dissolved in 100ml of 95% EtOH) for 5 minutes for cytoplasm staining, and then washed by cool-running water. Sections were dehydrated in graded ethanol for 5 minutes each time and then treated in xylene for 10 minutes and mounted with neutral gum for observation.

Magnetic resonance imaging (MRI)

The magnetic resonance images of orthotopic HCC mice were acquired using T2 propeller sequence with the following parameters: slice thickness of 1.0mm, slice spacing of 0.5mm, TR/TE of 3494/70.7ms, matrix of 256x160 and FOV of 8x8 cm (3.0 Tesia MR scanner, Signa Excite HDx; GE healthcare, Milwaukee, WI, US) with a small animal coil in Tianjin Medical University General Hospital. During the examination, mice were anesthetized with pentobarbital sodium and fixed to minimize body motion.

RS-OXA synthesis and Immunocytochemistry

RS-OXA [Pt(1R,2R-DACH)(ox)(suc)(sucRS)] were synthesized by China Peptides (Shanghai, China). For cellular co-localization, AF680-labeled RS-OXA (5 μM) were incubated with HL7702 or MHCC-LM3 cells for 24 h, followed by fixation with 4% PFA for 30 minutes at 4 °C and counterstaining with DAPI for 15 minutes at room temperature (RT). To examine the translocation of nucleophosmin (NPM1), HL7702 or MHCC-LM3 cells were treated with 5 μM RS-OXA or OXA for 24 h, and fixed with 4% PFA for 30 minutes at 4°C, followed by permeabilization with 0.1% Triton X-100 for 30 minutes and blocking with 5% goat serum for 2 h at RT. Subsequently, cells were stained with primary rabbit monoclonal antibody to NPM1 (1:100, Abcam, UK) at 4°C overnight, and then stained with Alexa Fluor 594-conjugated goat anti-rabbit secondary antibody (1:200; Molecular Probes, Thermo Scientific, US) in PBS with Tween 20 (PBST) for 1 h at RT, followed by counterstaining with DAPI for 15 minutes at RT. Cells were photographed using a confocal laser scanning microscope (LSM700, Carl Zeiss, Germany).

Annexin V and propidium iodide (PI) staining

OXA- and RS-OXA-induced cell apoptosis was measured with an Annexin V and Propidium Iodide (PI) Apoptosis Analysis Kit (Tianjin Sungene Biotech Co, Tianjin, China) as per manufacturer's instructions. Briefly, HL7702 or MHCC-LM3 cells (1×10^6) were cultured in 6-well plates overnight and treated with RS-OXA or OXA (10 μM) at 37°C for 36 h. Subsequently, cells were rinsed twice with cold PBS and trypsinized (without EDTA) for collection. The collected cells were resuspended in 250 μL of 1× binding buffer and stained with Annexin V-FITC in the dark at 25°C for 15 minutes, followed by incubation with 5 μL of 5 μM PI prior to flow cytometry (BD FACS Calibur; BD, Franklin Lakes, NJ, US).

3-(4,5-dimethylthiazol-2-yl)-2,5-diphenyltetrazolium bromide (MTT) assay

MTT assay was applied to determine the cytotoxic effect of RS-OXA *in vitro*.[50] Briefly, HL7702 and MHCC-LM3 cells were cultured in 96-well plates (2000 cells per well) for 24 h prior to treatment with OXA or RS-OXA at different concentrations (5, 10, 20, 40 and 80 μM) for 48 h. Subsequently, 10 μL of MTT (5 mg/mL in PBS) was added to each well for 4 h, and then the medium was replaced with DMSO (100 μL) for measurement. The samples were measured at 570nm using an enzyme-linked immunosorbent assay (ELISA) reader (Tecan, Sunrise, Switzerland).

Transwell assay

Transwell assays were performed to determine tumor cell invasion with Millipore Transwell chambers (8 μm pore size, Millipore, MA, US) coated with 1 mg/ml Matrigel (Corning, US). HL7702 and MHCC-LM3 cells were treated with 5 μM OXA or RS-OXA for 24 h prior to seeding in the upper chamber of a 12-well plate (3×10^4 per well) (Corning, US) in 500 μl serum-free medium and the lower chambers were filled with 1 ml complete medium and incubated at 37 °C for 24 h. Subsequently, cells at the upper surface of the membrane were removed with a cotton swab and the cells in the lower surface of the membrane were stained with 1% crystal violet for 15 minutes (Solarbio, China). Images were taken with an inverted microscope (Olympus BX51, Japan) and analyzed using ImageJ software (NIH, Bethesda, US).

Behavioral and toxicity tests

BALB/C nude mice were treated with PBS, OXA or RS-OXA (10 μmol/kg) for 5 times every 3 days apart. Bodyweight was recorded every two days after treatment. Events related to pain were recorded 24 h after the 5^{th} injection. Mice were placed on the Cold Plate (model 35100; Ugo Basile, Italy) at 4°C, and were free to move. The number of pain signs including rear licking and shaking, jumping, alterations in rear and tail movements was recorded consecutively for 5 minutes. After the cold-elicited behavioral tests, mice were sacrificed by cervical dislocation and liver/ kidney were harvested for histological examination.

Measurement of Pt in tissues

Tumor and liver tissues of orthotopic HCC mice were lyophilized and grinded with each 0.1 g tissue digested with HNO_3 (65%) at 65°C for 10 minutes, and the level of Pt in tissues were measured by

Inductively coupled plasma-mass spectrometry (ICP-MS) (Optima 5300DV, PerkinElmer, US).

Statistical analysis

All data are reported as mean values± SEM. Statistical differences between different groups were evaluated by SigmaStat (SystatSoftware, Inc, USA) with significance set at $p<0.05$. Both parametric and nonparametric analyses were applied as specified in Figure legends. Sample size was determined by PASS software (version 11; NCSS, UT, US).

Abbreviations

NSCLC
Non-small-cell lung cancer
SCLC
Small-cell lung cancer
HCC
Hepatocellular carcinoma
MDR
multidrug resistance
ABC
ATP-binding cassette
pI
isoelectric point
LC-MS
liquid chromatography-electrospray mass spectrometric
AST
aspartate aminotransferase
ALT
alanine aminotransferase
ICC
intrahepatic cholangiocarcinoma
NPM1
nucleophosmin
SOS
sinusoidal obstruction syndrome
PET
positron emission tomography
DMF
N,N-dimethylformamide
CA
colon adenocarcinoma

RS-OXA
[Pt(1R,2R-DACH)(ox)(suc)(sucRS)]
PBST
PBS with Tween 20

Declarations

Ethical Approval and Consent to participate

The mice experiments were carried out in the Animal unit, Tianjin Medical University (Tianjin, China), according to procedures authorized by the institutional ethical committee (Permit Number: SYXK 2019-0004).

The hepatocellular carcinoma (HCC), intrahepatic cholangiocarcinoma (ICC), combined HCC and ICC, colon adenocarcinoma (CA) and NSCLC patient biopsies used in this study were provided by Tianjin Medical University General Hospital and Cancer Hospital (Permit Number: bc2020175). The study was conducted in accordance with Declaration of Helsinki and was approved by the Tianjin Medical University Cancer Hospital Ethics Committee.

Consent for publication

All authors are content with and have agreed to submission of this manuscript to Molecular Cancer for publication.

Availability of supporting data

All data supporting this study are available within this article and supplementary Information file.

Competing interests

H.Y., R.J. and R.L. file a patent (202110167783.2). The authors declare no competing financial interests.

Funding

This study was supported by National Natural Science Foundation of China (no. 82030054), Natural Science Foundation of Tianjin (20JCQNJC00580), and Tianjin Municipal 13th five-year plan (Tianjin Medical University Talent Project).

Authors' contributions

H.Y. designed the project; R.J., Q.W., R.L., L.Z., X.Q., J.X., and B.Z. carried out the experiments; L.C., G.L., H.Z, J.C. and T.S helped with clinical sample collection; Y.S. helped with *in vitro* patient sample experiments; R.J. and H.Y. analyzed the data; H.Y. and R.J wrote the paper with the input from all authors.

Acknowledgements

We thank Core facility of Research Center of Basic Medical Sciences (Tianjin Medical University) for technical support, specifically the animal imaging core facilities.

Authors' information

Renwei Jing and Qian Wang contributed equally to this work.

Affiliations

The Province and Ministry Co-sponsored Collaborative Innovation Center for Medical Epigenetics & Department of Cell Biology & School of Medical Technology, Tianjin Medical University, Qixiangtai Road, Heping District, Tianjin, 300070, China

Renwei Jing, Qian Wang, Ruibin Li, Leijie Zhang, Bingfeng Zuo, HaiFang Yin.

Department of Genetics & Cancer Institute and Hospital, Tianjin Medical University, Tianjin 300070, China

Lu Chen, Guangtao Li, Tianqiang Song.

Department of Lung Cancer Surgery, Tianjin Medical University General Hospital, Tianjin 300070, China

Hongbing Zhang, Jun Chen.

Institute of Bioengineering and Bioimaging, 31 Biopolis Way, 138669, Singapore

Yiqi Seow.

Institute of Molecular and Cell Biology, 61 Biopolis Way, 138668, Singapore.

Yiqi Seow.

Tianjin Key Laboratory on Technologies Enabling Development of Clinical Therapeutics and Diagnostics, School of Pharmacy, Tianjin Medical University, Qixiangtai Road, Heping District, Tianjin, 300070, China.

Xin Qiao, Jingyuan Xu.

References

1. Cao R, Liu H, Cheng Z: **Radiolabeled Peptide Probes for Liver Cancer Imaging**. Curr Med Chem 2020, **27**:6968–6986.
2. Scodeller P, Asciutto EK: **Targeting Tumors Using Peptides**. Molecules 2020, **25**.
3. Burggraaf J, Kamerling IM, Gordon PB, Schrier L, de Kam ML, Kales AJ, Bendiksen R, Indrevoll B, Bjerke RM, Moestue SA, et al: **Detection of colorectal polyps in humans using an intravenously administered fluorescent peptide targeted against c-Met**. Nat Med 2015, **21**:955–961.

4. Ongarora BG, Fontenot KR, Hu X, Sehgal I, Satyanarayana-Jois SD, Vicente MG: **Phthalocyanine-peptide conjugates for epidermal growth factor receptor targeting**. J Med Chem 2012, **55**:3725–3738.
5. Wang Q, Li SB, Zhao YY, Dai DN, Du H, Lin YZ, Ye JC, Zhao J, Xiao W, Mei Y, et al: **Identification of a sodium pump Na(+)/K(+) ATPase alpha1-targeted peptide for PET imaging of breast cancer**. J Control Release 2018, **281**:178–188.
6. Lang FF, Conrad C, Gomez-Manzano C, Yung WKA, Sawaya R, Weinberg JS, Prabhu SS, Rao G, Fuller GN, Aldape KD, et al: **Phase I Study of DNX-2401 (Delta-24-RGD) Oncolytic Adenovirus: Replication and Immunotherapeutic Effects in Recurrent Malignant Glioma**. Journal of Clinical Oncology 2018, **36**:1419-+.
7. Zuo HD: **iRGD**: **A Promising Peptide for Cancer Imaging and a Potential Therapeutic Agent for Various Cancers**. *Journal of Oncology* 2019, **2019**.
8. Sani S, Messe M, Fuchs Q, Pierrevelcin M, Laquerriere P, Entz-Werle N, Reita D, Etienne-Selloum N, Bruban V, Choulier L, et al: **Biological Relevance of RGD-Integrin Subtype-Specific Ligands in Cancer**. Chembiochem 2021, **22**:1151–1160.
9. Katsamakas S, Chatzisideri T, Thysiadis S, Sarli V: **RGD-mediated delivery of small-molecule drugs**. Future Medicinal Chemistry 2017, **9**:579–604.
10. Zhu L, Ding Z, Li X, Wei H, Chen Y: **Research Progress of Radiolabeled Asn-Gly-Arg (NGR) Peptides for Imaging and Therapy**. Mol Imaging 2020, **19**:1536012120934957.
11. Kis A, Denes N, Szabo JP, Arato V, Joszai I, Enyedi KN, Lakatos S, Garai I, Mezo G, Kertesz I, Trencsenyi G: **In vivo assessment of aminopeptidase N (APN/CD13) specificity of different (68)Ga-labelled NGR derivatives using PET/MRI imaging**. Int J Pharm 2020, **589**:119881.
12. Zucali PA, Simonelli M, De Vincenzo F, Lorenzi E, Perrino M, Bertossi M, Finotto R, Naimo S, Balzarini L, Bonifacio C, et al: **Phase I and pharmacodynamic study of high-dose NGR-hTNF in patients with refractory solid tumours**. British Journal of Cancer 2013, **108**:58–63.
13. Hein N, Hannan KM, George AJ, Sanij E, Hannan RD: **The nucleolus: an emerging target for cancer therapy**. Trends in Molecular Medicine 2013, **19**:643–654.
14. Lafontaine DLJ, Riback JA, Bascetin R, Brangwynne CP: **The nucleolus as a multiphase liquid condensate**. Nature Reviews Molecular Cell Biology 2021, **22**:165–182.
15. Pickard AJ, Bierbach U: **The Cell's Nucleolus: an Emerging Target for Chemotherapeutic Intervention**. Chemmedchem 2013, **8**:1441–1449.
16. Rhee M, Davis P: **Mechanism of uptake of C105Y, a novel cell-penetrating peptide**. Journal of Biological Chemistry 2006, **281**:1233–1240.
17. Xu JK, Khan AR, Fu MF, Wang RJ, Ji JB, Zhai GX: **Cell-penetrating peptide: a means of breaking through the physiological barriers of different tissues and organs**. Journal of Controlled Release 2019, **309**:106–124.
18. Marian T, Szabo G, Goda K, Nagy H, Szincsak N, Juhasz I, Galuska L, Balkay L, Mikecz P, Tron L, Krasznai Z: **In vivo and in vitro multitracer analyses of P-glycoprotein expression-related multidrug**

resistance. Eur J Nucl Med Mol Imaging 2003, **30**:1147–1154.

19. Livshits Z, Rao RB, Smith SW: **An approach to chemotherapy-associated toxicity**. Emerg Med Clin North Am 2014, **32**:167–203.
20. Ikeda M, Morizane C, Ueno M, Okusaka T, Ishii H, Furuse J: **Chemotherapy for hepatocellular carcinoma: current status and future perspectives**. Japanese Journal of Clinical Oncology 2018, **48**:103–114.
21. Ivanusic D, Madela K, Bannert N, Denner J: **The large extracellular loop of CD63 interacts with gp41 of HIV-1 and is essential for establishing the virological synapse**. Sci Rep 2021, **11**:10011.
22. Qin SK, Bai YX, Lim HY, Thongprasert S, Chao Y, Fan J, Yang TS, Bhudhisawasdi V, Kang WK, Zhou Y, et al: **Randomized, Multicenter, Open-Label Study of Oxaliplatin Plus Fluorouracil/Leucovorin Versus Doxorubicin As Palliative Chemotherapy in Patients With Advanced Hepatocellular Carcinoma From Asia**. Journal of Clinical Oncology 2013, **31**:3501-+.
23. Hsu HH, Chen MC, Baskaran R, Lin YM, Day CH, Lin YJ, Tu CC, Padma VV, Kuo WW, Huang CY: **Oxaliplatin resistance in colorectal cancer cells is mediated via activation of ABCG2 to alleviate ER stress induced apoptosis**. Journal of Cellular Physiology 2018, **233**:5458–5467.
24. Argyriou AA, Polychronopoulos P, Iconomou G, Chroni E, Kalofonos HP: **A review on oxaliplatin-induced peripheral nerve damage**. Cancer Treat Rev 2008, **34**:368–377.
25. Bruno PM, Liu YP, Park GY, Murai J, Koch CE, Eisen TJ, Pritchard JR, Pommier Y, Lippard SJ, Hemann MT: **A subset of platinum-containing chemotherapeutic agents kills cells by inducing ribosome biogenesis stress**. Nature Medicine 2017, **23**:461-+.
26. Sutton EC, McDevitt CE, Prochnau JY, Yglesias MV, Mroz AM, Yang MC, Cunningham RM, Hendon CH, DeRose VJ: **Nucleolar Stress Induction by Oxaliplatin and Derivatives**. Journal of the American Chemical Society 2019, **141**:18411–18415.
27. Jing R, Zhou X, Zhao J, Wei Y, Zuo B, You A, Rao Q, Gao X, Yang R, Chen L, et al: **Fluorescent peptide highlights micronodules in murine hepatocellular carcinoma models and humans in vitro**. Hepatology 2018, **68**:1391–1411.
28. Sharma A, Kapoor P, Gautam A, Chaudhary K, Kumar R, Chauhan JS, Tyagi A, Raghava GP: **Computational approach for designing tumor homing peptides**. Sci Rep 2013, **3**:1607.
29. Ruseska I, Zimmer A: **Internalization mechanisms of cell-penetrating peptides**. Beilstein J Nanotechnol 2020, **11**:101–123.
30. Shindoh J, Hasegawa K, Inoue Y, Ishizawa T, Nagata R, Aoki T, Sakamoto Y, Sugawara Y, Makuuchi M, Kokudo N: **Risk factors of post-operative recurrence and adequate surgical approach to improve long-term outcomes of hepatocellular carcinoma**. HPB (Oxford) 2013, **15**:31–39.
31. Rao Q, You A, Guo Z, Zuo B, Gao X, Zhang T, Du Z, Wu C, Yin H: **Intrahepatic Tissue Implantation Represents a Favorable Approach for Establishing Orthotopic Transplantation Hepatocellular Carcinoma Mouse Models**. PLoS One 2016, **11**:e0148263.
32. Qi S, Zhang Y, Liu G, Chen J, Li X, Zhu Q, Yang Y, Wang F, Shi J, Lee CS, et al: **Plasmonic-doped melanin-mimic for CXCR4-targeted NIR-II photoacoustic computed tomography-guided photothermal**

ablation of orthotopic hepatocellular carcinoma. Acta Biomater 2021, **129**:245–257.

33. Chen RX, Song HY, Dong YY, Hu C, Zheng QD, Xue TC, Liu XH, Zhang Y, Chen J, Ren ZG, et al: **Dynamic expression patterns of differential proteins during early invasion of hepatocellular carcinoma**. PLoS One 2014, **9**:e88543.
34. Chan JK: **The wonderful colors of the hematoxylin-eosin stain in diagnostic surgical pathology**. Int J Surg Pathol 2014, **22**:12–32.
35. Sethi D, Sen R, Parshad S, Khetarpal S, Garg M, Sen J: **Histopathologic changes following neoadjuvant chemotherapy in various malignancies**. Int J Appl Basic Med Res 2012, **2**:111–116.
36. Yoshida Y, Nitadori JI, Shinozaki-Ushiku A, Sato J, Miyaji T, Yamaguchi T, Fukayama M, Nakajima J: **Micropapillary histological subtype in lung adenocarcinoma of 2 cm or less: impact on recurrence and clinical predictors**. Gen Thorac Cardiovasc Surg 2017, **65**:273–279.
37. Travis WD, Brambilla E, Noguchi M, Nicholson AG, Geisinger KR, Yatabe Y, Beer DG, Powell CA, Riely GJ, Van Schil PE, et al: **International association for the study of lung cancer/american thoracic society/european respiratory society international multidisciplinary classification of lung adenocarcinoma**. J Thorac Oncol 2011, **6**:244–285.
38. Kadota K, Nitadori J, Woo KM, Sima CS, Finley DJ, Rusch VW, Adusumilli PS, Travis WD: **Comprehensive pathological analyses in lung squamous cell carcinoma: single cell invasion, nuclear diameter, and tumor budding are independent prognostic factors for worse outcomes**. J Thorac Oncol 2014, **9**:1126–1139.
39. Jaimes N, Zalaudek I, Braun RP, Tan BH, Busam KJ, Marghoob AA: **Pearls of keratinizing tumors**. Arch Dermatol 2012, **148**:976.
40. Rieger AM, Nelson KL, Konowalchuk JD, Barreda DR: **Modified annexin V/propidium iodide apoptosis assay for accurate assessment of cell death**. J Vis Exp 2011.
41. Wang Z, Zhou J, Fan J, Qiu SJ, Yu Y, Huang XW, Sun J, Tan CJ, Dai Z: **Oxaliplatin induces apoptosis in hepatocellular carcinoma cells and inhibits tumor growth**. Expert Opin Investig Drugs 2009, **18**:1595–1604.
42. Zhang Y, Yonezawa A, Nakagawa S, Imai S, Denda M, Omura T, Nakagawa T, Matsubara K: **Cisplatin, rather than oxaliplatin, increases paracellular permeability of LLC-PK1 cells via activating protein kinase C**. Drug Metab Pharmacokinet 2020, **35**:111–116.
43. Staff NP, Cavaletti G, Islam B, Lustberg M, Psimaras D, Tamburin S: **Platinum-induced peripheral neurotoxicity: From pathogenesis to treatment**. J Peripher Nerv Syst 2019, **24 Suppl 2**:S26-S39.
44. Duwe G, Knitter S, Pesthy S, Beierle AS, Bahra M, Schmelzle M, Schmuck RB, Lohneis P, Raschzok N, Ollinger R, et al: **Hepatotoxicity following systemic therapy for colorectal liver metastases and the impact of chemotherapy-associated liver injury on outcomes after curative liver resection**. Eur J Surg Oncol 2017, **43**:1668–1681.
45. Leung J, Ball D, Worotniuk T, Laidlaw C: **Survival following radiotherapy for post-surgical locoregional recurrence of non-small cell lung cancer**. Lung Cancer 1995, **13**:121–127.

46. Gately L, Jalali A, Semira C, Faragher I, Croxford M, Ananda S, Kosmider S, Field K, Lok SW, Gard G, et al: **Stage dependent recurrence patterns and post-recurrence outcomes in non-metastatic colon cancer**. Acta Oncol 2021, **60**:1106–1113.
47. Calandri M, Gazzera C, Yevich S, Lapenna K, Marenco M, Veltri A, Paraluppi G, Fonio P: **Post-surgical recurrence of hepatocellular carcinoma along resection margin treated by percutaneous US-guided ablation**. Minerva Chir 2018, **73**:255–260.
48. Lai Y, Lee JC, Hung HC, Cheng CH, Wu TH, Lee CF, Wu TJ, Chou HS, Chan KM, Lee WC: **Models to predict disease-free survival for hepatocellular carcinoma patients with surgical resections**. J Surg Oncol 2020, **122**:1444–1452.
49. Roberts LR, Sirlin CB, Zaiem F, Almasri J, Prokop LJ, Heimbach JK, Murad MH, Mohammed K: **Imaging for the diagnosis of hepatocellular carcinoma: A systematic review and meta-analysis**. Hepatology 2018, **67**:401–421.
50. Fu XT, Song K, Zhou J, Shi YH, Liu WR, Shi GM, Gao Q, Wang XY, Ding ZB, Fan J: **Tumor-associated macrophages modulate resistance to oxaliplatin via inducing autophagy in hepatocellular carcinoma**. Cancer Cell Int 2019, **19**:71.

Figures

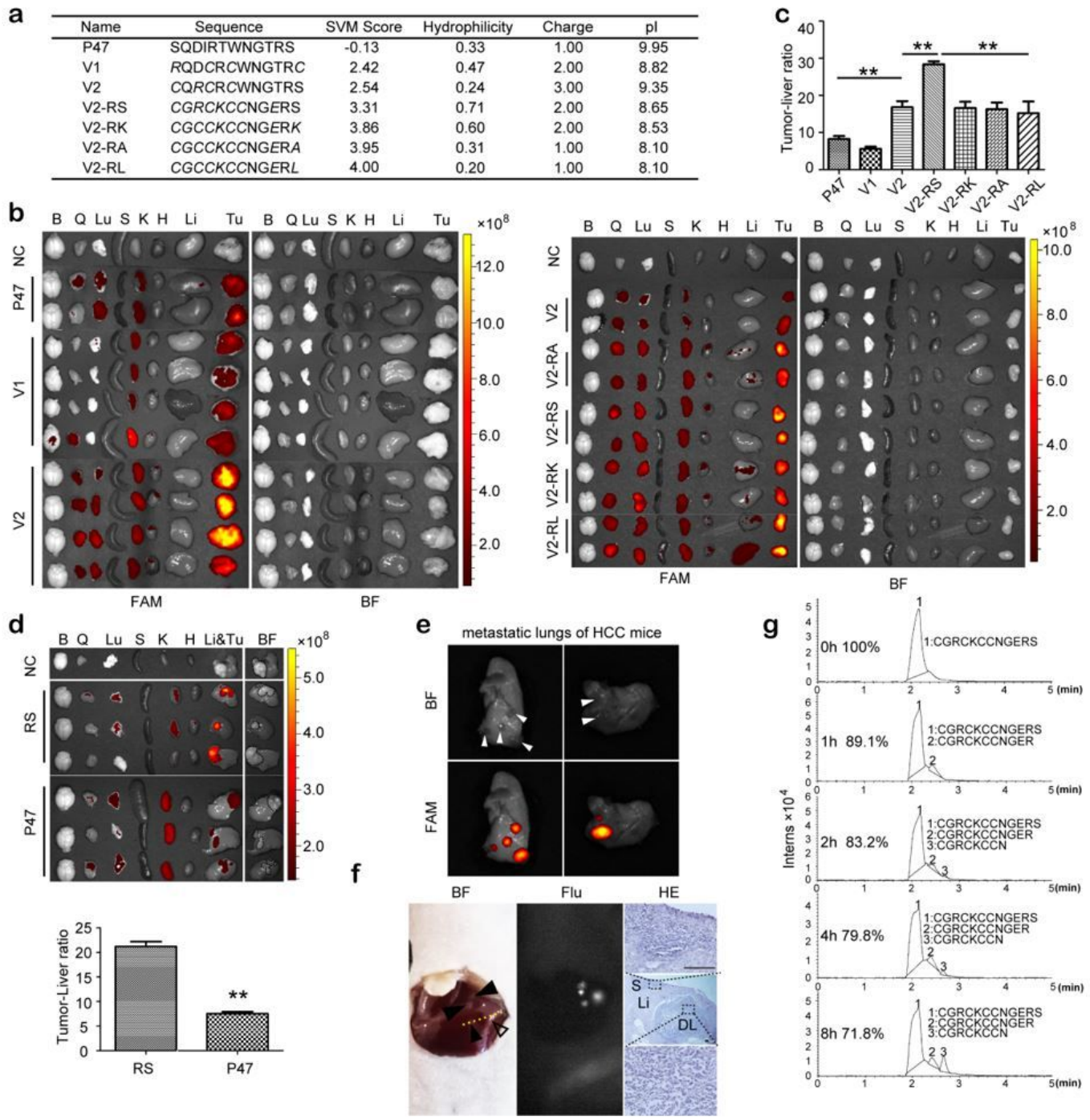

Figure 1

Identification and evaluation of lead peptide (RS) *in vivo*. (**a**) Nomenclature and sequence of P47 variants (V). Italic letters represent mutated amino acids. (**b**) Tissue distribution of FAM-labeled P47, V1, V2, V2-RA, V2-RS, V2-RK and V2-RL peptides in *C57BL/6* mice bearing subcutaneous HCC tumors. FAM-labeled peptides were intravenously administered into subcutaneous HCC mice at the dose of 25 mg/kg for single injection. Tissues were harvested 2 h after injection. B-brain; Q-quadriceps; Lu-lung; S-spleen; K-kidney; H-heart; Li-liver; Tu-tumor; NC-negative control (mice injected with buffer). (**c**) Quantitative analysis of the tumor/ liver ratio of mice injected with P47 (n=4), V1 (n=4), V2 (n=6), V2-RS (n=3), V2-RK (n=3), V2-

RA (n=3) and V2-RL (n=3) peptides (**p<0.01, One way-ANOVA post hoc Student-Newman-Keuls test). (**d**) Tissue distribution and quantitative analysis of FAM-labeled RS and P47 peptides in orthotopic HCC mice (n=3; **p<0.01, two-tailed t test). FAM-labeled peptides were intravenously administered to mice bearing orthotopic HCC or lung metastatic HCC nodules in lung at the dose of 25 mg/kg for single injection. Tissues were harvested 2 h after injection. The abbreviation for tissues harvested is the same as above. (**e**) Delineation of metastatic HCC micronodules in lungs of mice with FAM-labeled RS. Arrowheads point to metastatic micronodules in lung of *C57BL/6* mice. (**f**) Detection of deeply-located micronodules in the liver of mice bearing human orthotopic HCC tumors. RS modified with quantum dot (Ag_2S-RS) was injected intravenously into mice bearing human orthotopic HCC tumors at the dose of 4 mg/kg for single injection and mice were monitored in situ with a NIR-II image system. Black and white arrowheads indicate tumors on the surface of or deep inside the liver, respectively. The dotted line refers to the area for pathological examination (scale bar=100 μm). S-Superficial; DL- Deeply-located. (**g**) Liquid chromatographic-mass spectrometric (LC-MS) analysis of RS stability in 20% of serum. BF-Bright Field; Flu-fluorescence.

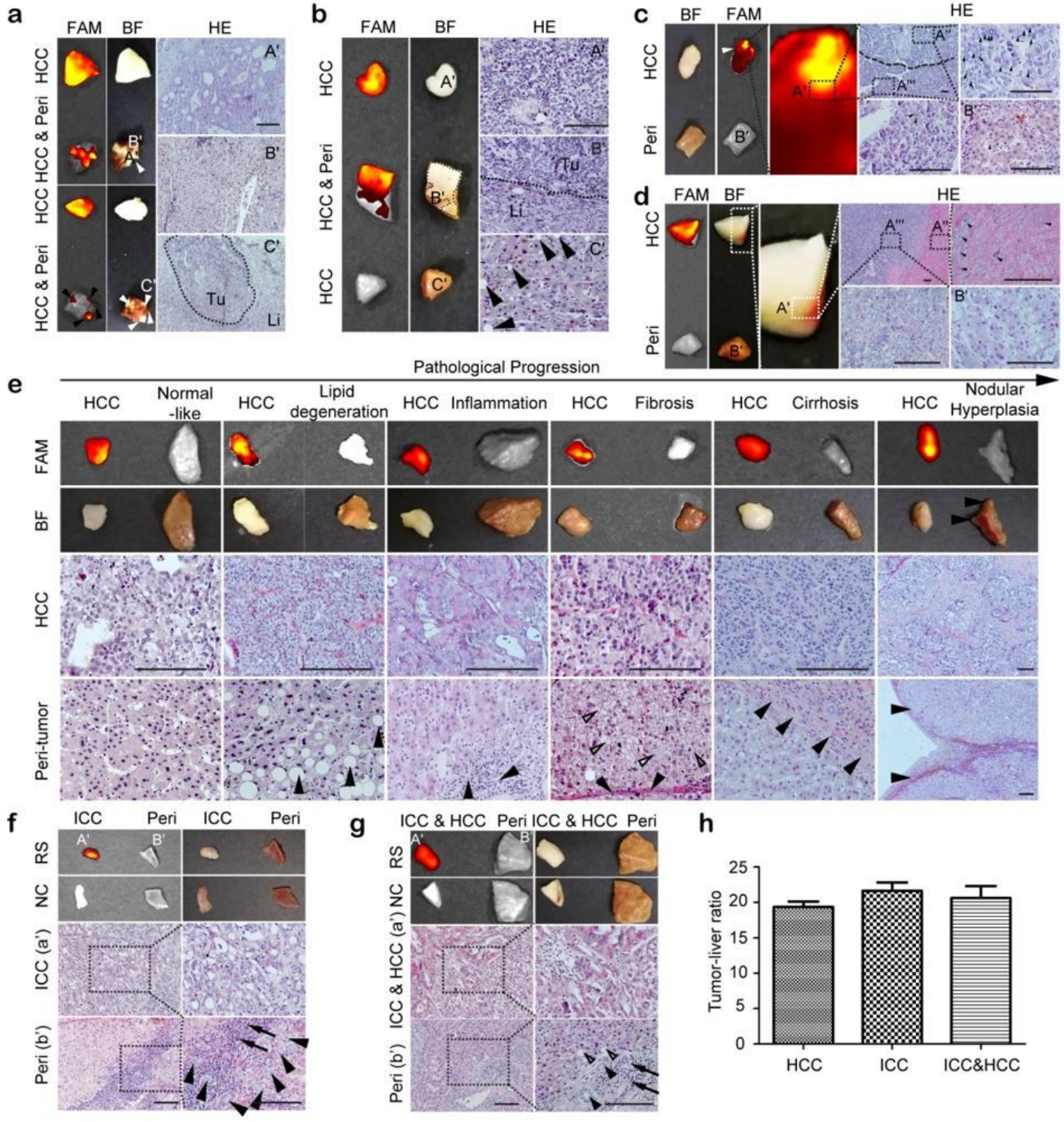

Figure 2

Evaluation of RS peptide in liver cancer patient biopsies. (**a**) Staining of HCC patient tissues with micronodules by FAM-labeled RS peptide. Peri-peritumoral; A' for tumor; B' for peritumoral liver; C' for micronodules; Tu-tumor; Li-liver. (**b**) Staining of HCC patient tissues with tumor infiltration by FAM-labeled RS peptide. A' for tumor; B' for the boundary of tumor and liver with tumor infiltration; C' for peritumoral liver. Black arrowheads point to lipid bubbles. (**c**) Staining of HCC patient tumor biopsies with different proliferative activities by FAM-labeled RS peptide. A' for tumor cells containing basophilic (A") and

acidophilic (A‴) cytoplasm; B’ for peritumoral liver. (**d**) Staining of HCC patient biopsies with hemorrhagic necrosis by FAM-labeled RS peptide. A’ includes tumor (A‴) with hemorrhagic necrosis (A″); B’ for peritumoral liver. (**e**) Evaluation of RS peptide in HCC patient biopsies with different stages of liver pathologies in the order of disease progression. Black arrowheads point to lipid bubbles, inflammatory infiltration, moderate hepatic fibrosis, severe hepatic fibrosis, and regenerative nodules, respectively. Hollow arrowheads in fibrosis point to ground-glass hepatocytes. (**f**) Staining of patient biopsies with intrahepatic cholangiocarcinoma (ICC) by FAM-labeled RS peptide. A’ for ICC; B’ for peritumoral liver. Black arrows point to inflammatory cells; black arrowheads point to intrahepatic bile ducts with excessive proliferation. (**g**) Staining of patient biopsies with combined ICC and HCC by FAM-labeled RS peptide. Black arrows point to inflammatory cells; black arrowheads point to intrahepatic bile ducts; hollow arrowheads point to lipid bubbles. (**h**) Quantitative analysis of tumor/ liver ratios in HCC (n=14), ICC (n=3) and ICC&HCC (n=3) patient biopsies. Data are presented as mean± SEM (scale bar=100 μm).

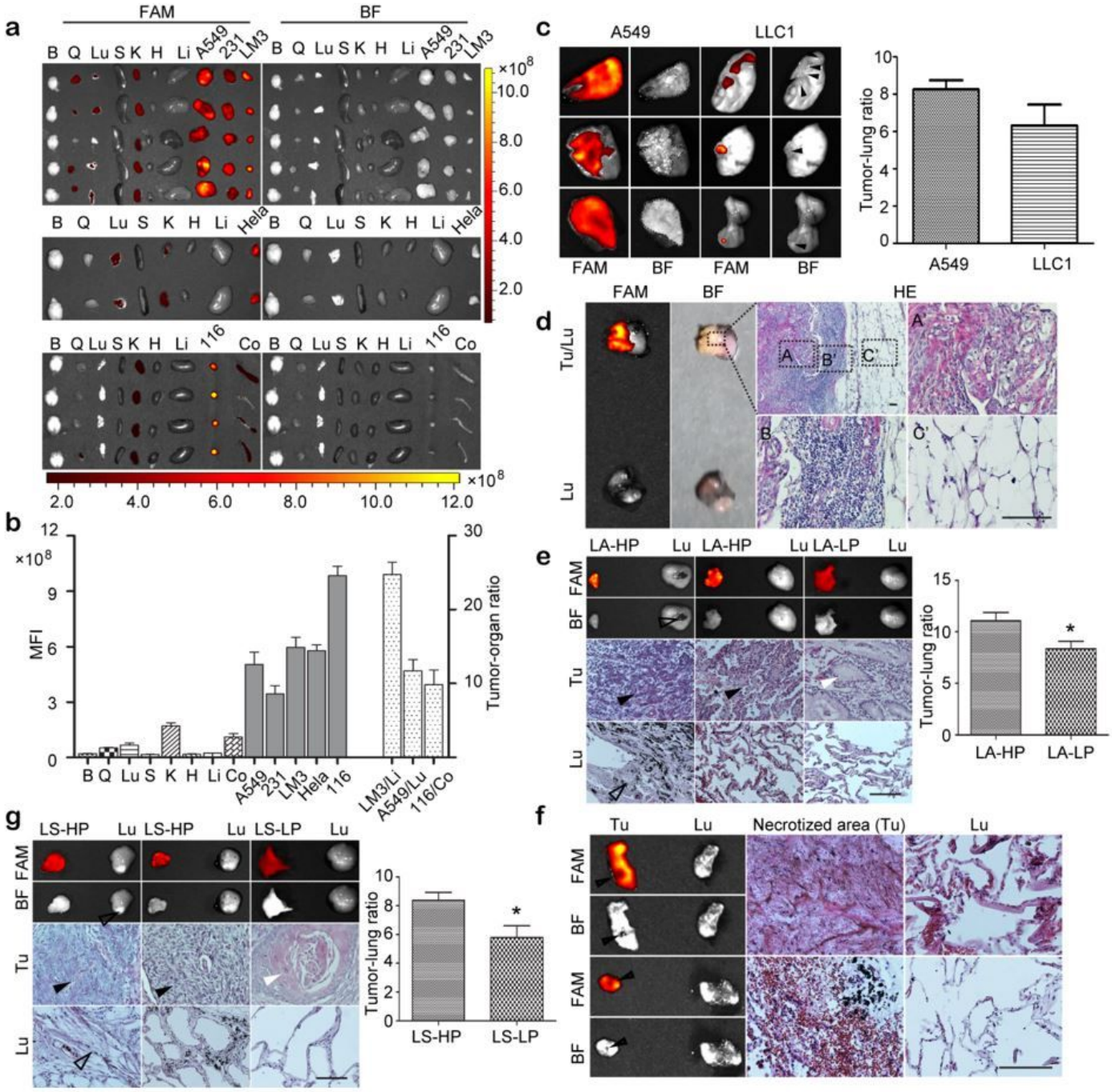

Figure 3

Evaluation of RS peptide in mice and patient biopsies with other tumors. (**a**) Tissue distribution of FAM-labeled RS peptides in nude mice bearing subcutaneous tumors of human NSCLC, breast cancer, HCC, cervical cancer and colon cancer. (**b**) Quantitative analysis of mean fluorescence intensity (MFI) of different tissues after intravenous injection of FAM-labeled RS peptides. The tumor/ organ ratio refers to HCC/ liver, NSCLC/ lung and colon cancer/colon, respectively. (**c**) Visualization of NSCLC in lung of mice bearing murine (LLC1) and human (A549) NSCLC with FAM-labeled RS and quantitative analysis of the tumor/ lung ratio (n=3). (**d**) Staining of NSCLC patient biopsies with infiltrating monocytes by FAM-

labeled RS peptide. A’ for tumor; B’ for infiltrating monocytes; C for peritumoral lung tissues. (**e**) Staining of patient biopsies with lung adenocarcinoma of low (n=3) or high (n=4) proliferative activities by FAM-labeled RS peptide and quantitative analysis of the tumor/ lung ratio (*p < 0.05, two-tailed t test). LA-LP or -HP refers to lung adenocarcinoma with low or high proliferative activities. Black arrowheads point to papillary or micropapillary structures. White arrowhead points to simple acinar structures. Hollow arrowheads point to the pneumoconiosis. (**f**) Staining of lung adenocarcinoma patient biopsies with necrosis (scale bar=100 μm). Black arrowheads point to necrotized areas. (**g**) Staining of patient biopsies with lung squamous carcinoma of low (n=3) or high (n=5) proliferative activities by FAM-labeled RS peptide and quantitative analysis of the tumor/ lung ratio (*p<0.05, two-tailed t test). LS-LP or -HP refers to lung squamous carcinoma with low or high proliferative activities. Black arrowheads point to clustered tumor cells with high nucleo-cytoplasmic ratio. Hollow arrowheads point to fibrotic areas. The white arrowhead points to a keratin pearl at the center of cancer nest.

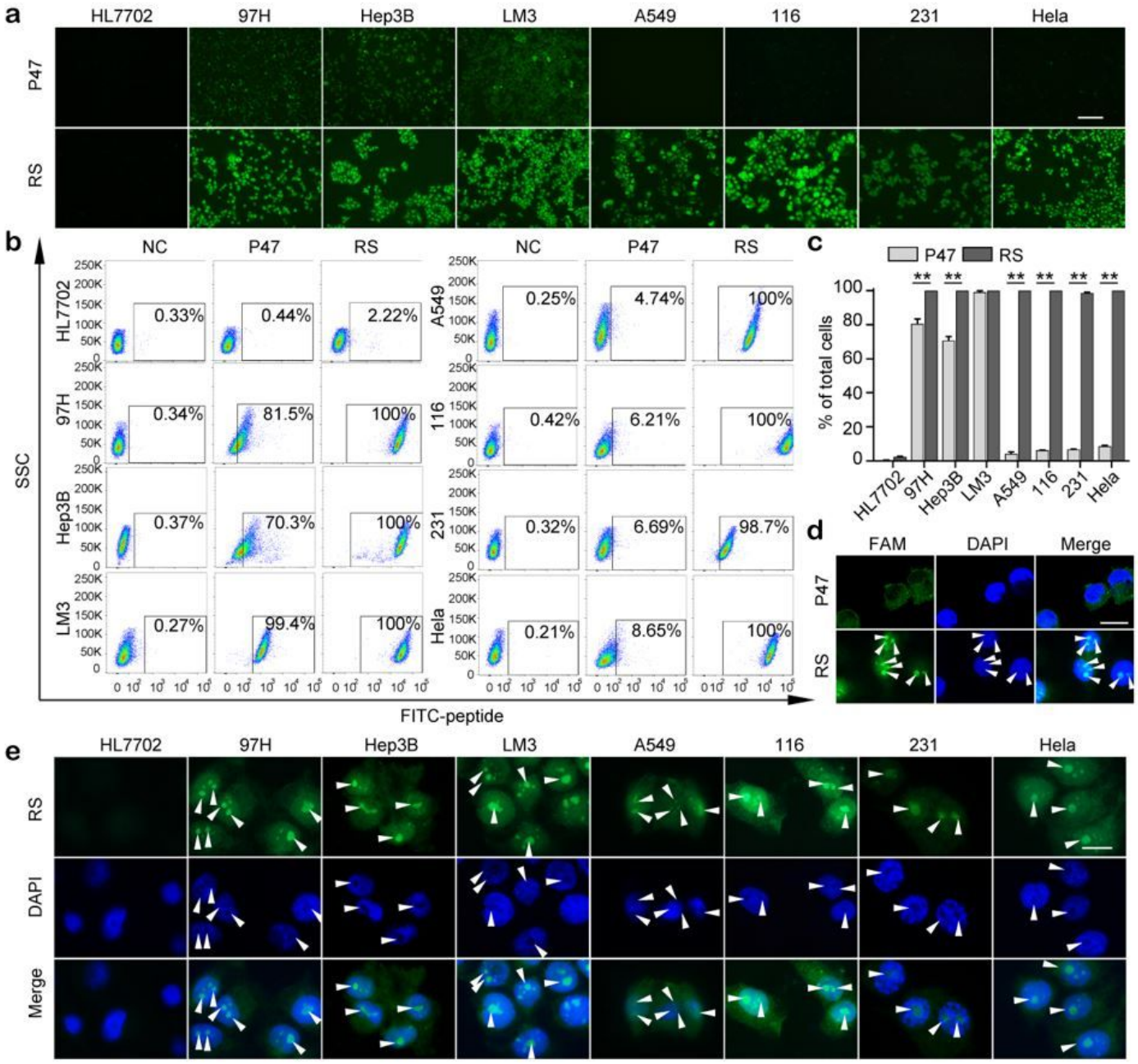

Figure 4

Cellular uptake and localization of FAM-labeled RS peptide *in vitro*. FAM-labeled RS and P47 peptides (2 μM) were incubated with different cells and observed 6 h later. (**a**) Cellular uptake of FAM-labeled RS and P47 peptides in HL7702, MHCC-97H, Hep3B, MHCC-LM3, A549, HCT116, MDA-MB-231 and Hela cells (scale bar=100 μm). Flow cytometry (**b**) and quantitative analysis (**c**) of cellular uptake of FAM-labeled RS and P47 peptides in different cells (n=3; **p<0.01, two-tailed t test). (**d**) Localization of FAM-labeled RS and P47 peptides in MHCC-97H cells (scale bar=10 μm). Cell nuclei were counterstained with DAPI (blue). (**e**) Localization of FAM-labeled RS peptide in HL7702, MHCC-97H, Hep3B, MHCC-LM3, A549, HCT116, MDA-MB-231 and Hela cells (scale bar=10 μm). White arrowheads point to cell nucleoli.

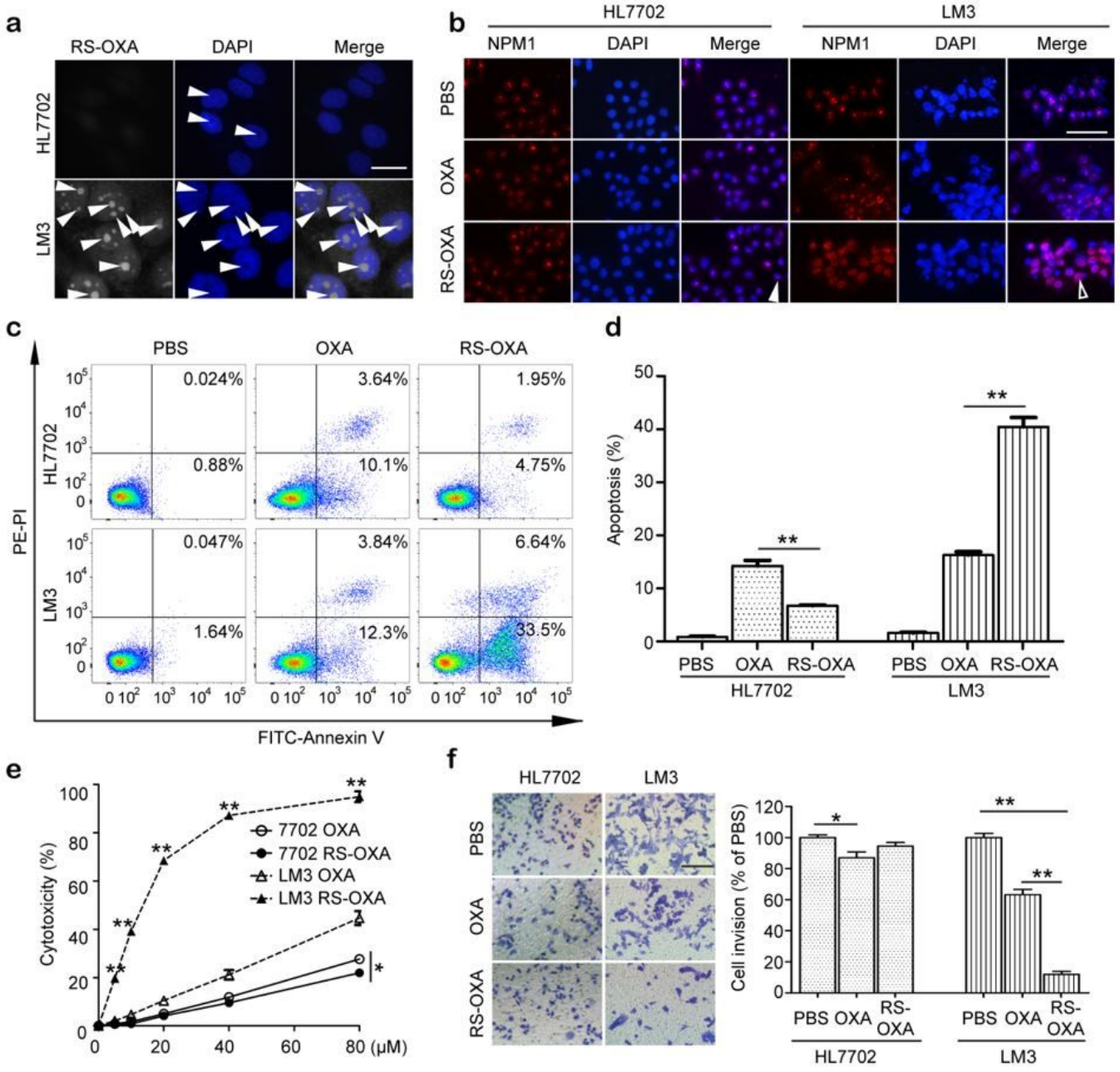

Figure 5

Assessment of RS modified OXA (RS-OXA) ***in vitro.*** (**a**) Cellular localization of AF680-labeled RS-OXA in HL7702 and MHCC-LM3 cells (scale bar=10 μm). White arrowheads point to cell nucleoli. (**b**) Immunocytochemistry for NPM1 in nucleoli and nucleoplasm of HL7702 and MHCCLM3 cells treated with RS-OXA. NPM1 (red) was stained 24 h after treatment with 5 μM OXA or RS-OXA. The white arrowhead points to NPM1 in nucleoli. The hollow arrowhead points to NPM1 relocalized in nucleoplasm of RS-OXA-treated MHCC-LM3 cells (scale bar=50 μm). (**c**) Immunocytochemistry of Annexin V-FITC and PI in MHCC-LM3 cells treated with 10 μM OXA or RS-OXA. HL7702 or MHCC-LM3 cells were treated with 10 μM OXA or RS-OXA for 36 h. (**d**) Quantitative analysis of the percentage of apoptotic cells relative to total cells treated with OXA or RS-OXA (n=3; **p<0.01, One way-ANOVA post hoc Student-Newman-Keuls

test). (**e**) Cytotoxic analysis of cells treated with OXA or RS-OXA at the concentrations of 5, 10, 20, 40 and 80 μM (n=3; *p<0.05, **p<0.01, One way-ANOVA post hoc Student- Newman-Keuls test). HL7702 or MHCC-LM3 cells were treated with different concentrations of OXA or RS-OXA for 48 h. (**f**) Transwell assay and quantitative analysis for invasion ability of cells treated with 5 μM OXA or RS-OXA (n=3; *p<0.05, **p<0.01, One way-ANOVA post hoc Student-Newman-Keuls test). HL7702 or MHCC-LM3 cells were treated with 5 μM OXA or RS-OXA for 24 h.

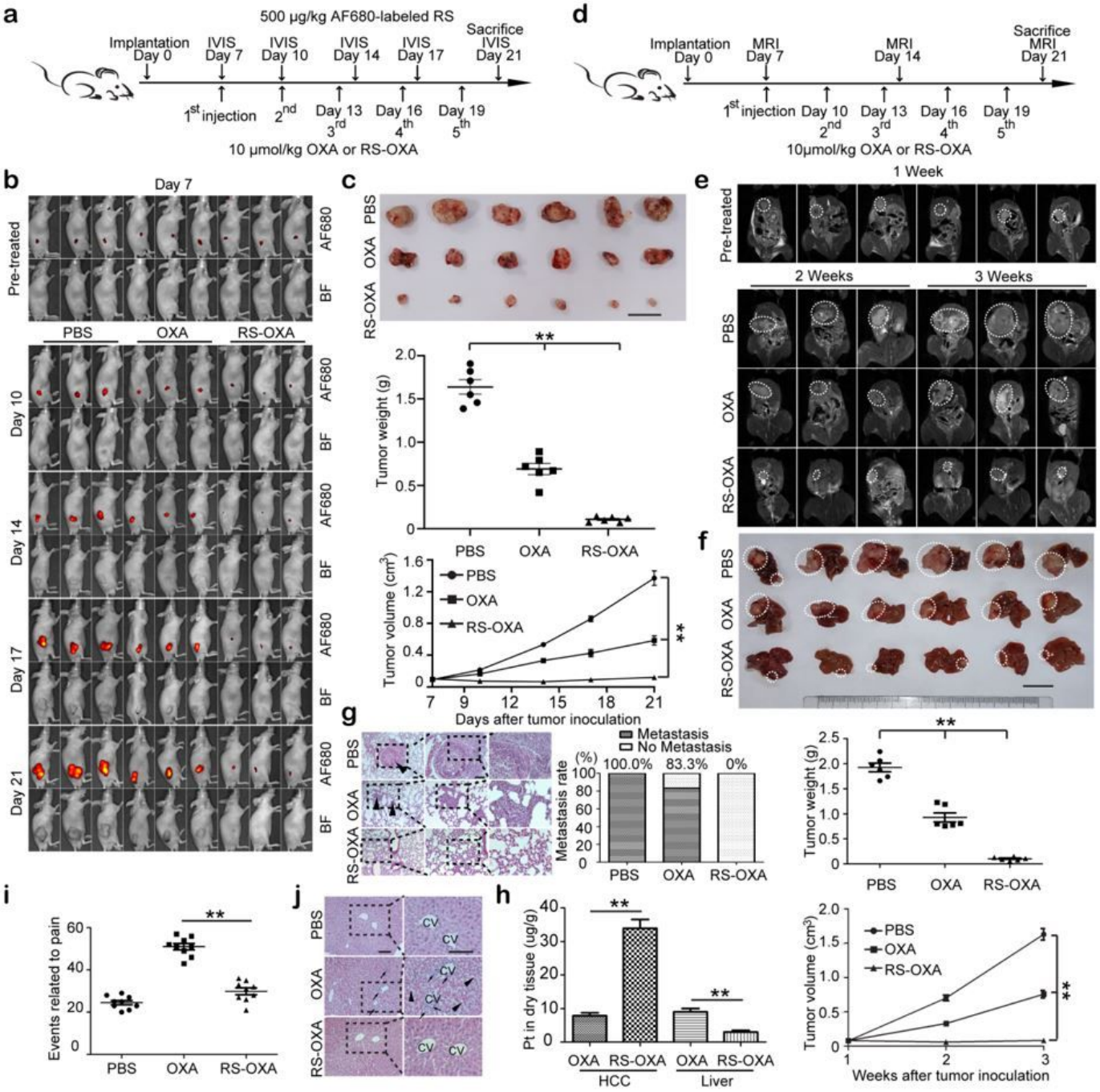

Figure 6

Systemic investigation of RS-OXA *in vivo*. (**a**) Schematic diagram for the dosing regimen of RS-OXA in day-7 subcutaneous HCC mice. (**b**) Real-time monitoring of tumor nodules in day-7 subcutaneous HCC mice treated with PBS, OXA or RS-OXA at different time-points. AF680-labeled RS peptides were intravenously injected into mice 12 h prior to imaging. (**c**) Representative tumor images and quantitative analysis of tumor weight and volume of subcutaneous HCC mice treated with PBS, OXA or RS-OXA (n=6; **p<0.01, One way-ANOVA post hoc Student-Newman-Keuls test). (**d**) Schematic diagram for the dosing regimen of RS-OXA in day-7 orthotopic HCC mice. (**e**) Real-time MRI monitoring of tumor growth in day-7 orthotopic HCC mice treated with PBS, OXA or RS-OXA at different time-points. Tumors were circled in the images. (**f**) Representative tumor images and quantitative analysis of tumor weight and volume of orthotopic HCC mice treated with PBS, OXA or RS-OXA (n=6; **p<0.01, One way-ANOVA post hoc Student-Newman-Keuls test). (**g**) Histological examination and quantitative analysis of pulmonary metastasis of HCC in lungs of orthotopic HCC mice treated with PBS, OXA or RS-OXA. (**h**) Quantification of Pt in tumor and liver of orthotopic HCC mice treated with OXA or RS-OXA (n=3; **p<0.01, two-tailed t test). (**i**) Measurement of events related to pain of wild-type nude mice treated with PBS, OXA or RS-OXA. Events related to pain were recorded 24 h after the fifth injection during cold stimulation (n=9; **p<0.01, One way-ANOVA post hoc Student-Newman-Keuls test). (**j**) Histological analysis of liver from wild-type nude mice treated with PBS, OXA or RS-OXA. Livers were harvested 2 days after the fifth injection. Arrows point to fibrotic areas in central vein (CV) and hepatic sinusoid. Arrowheads point to enlarged hepatic sinusoid (scale bar=100 μm).

Supplementary Files

This is a list of supplementary files associated with this preprint. Click to download.

- SupplementaryFigures.docx